Journal of Physics D: Applied Physics

PAPER

Second-harmonic signature of chiral spin structures in W/Pt/Co heterostructures with tunable magnetic anisotropy

To cite this article: Yang Wang *et al* 2023 *J. Phys. D: Appl. Phys.* **56** 205002

IOP Publishing Journal of Physics D: Applied Physics
J. Phys. D: Appl. Phys. **56** (2023) 205002 (7pp) https://doi.org/10.1088/1361-6463/acc40f

Second-harmonic signature of chiral spin structures in W/Pt/Co heterostructures with tunable magnetic anisotropy

Yang Wang[1], Ying-Ting Chan[2], Xiao Wang[3], Tao Wang[1], Xuemei M Cheng[3], Weida Wu[2] and John Q Xiao[1,*]

[1] Department of Physics and Astronomy, University of Delaware, Newark, DE 19716, United States of America
[2] Department of Physics and Astronomy, Rutgers University, Piscataway, NJ 08854, United States of America
[3] Department of Physics, Bryn Mawr College, Bryn Mawr, PA 19010, United States of America

E-mail: jqx@udel.edu

Received 6 October 2022, revised 20 February 2023
Accepted for publication 14 March 2023
Published 28 March 2023

Abstract

Second-harmonic Hall voltage (SHV) measurement method has been widely used to characterize the strengths of spin–orbit torques (SOTs) in heavy metal/ferromagnet thin films saturated in the single-domain regime. Here, we show that the magnetic anisotropy of a W/Pt/Co trilayer can be robustly tuned from in-plane to out-of-plane by varying W, Pt, or Co thicknesses. Moreover, in samples with easy-cone anisotropy, SHV measurements exhibit anomalous 'humps' in the multidomain regime accessed by applying a nearly out-of-plane external magnetic field. These hump features can only be explained as a result of the formation of Néel-type domain walls, efficiently driven by nevertheless small SOTs in this double heavy metal heterostructure with canceling spin Hall angles.

Keywords: second-harmonic Hall voltage measurement, chiral domain walls, Dzyaloshinskii–Moriya interaction, magnetic anisotropy

(Some figures may appear in colour only in the online journal)

1. Introduction

In magnetic thin films with perpendicular magnetic anisotropy (PMA), Bloch-type domain walls (DWs) are favored due to their smaller magnetostatic energies as compared to Néel-type DWs [1]. Because the exchange, magnetic anisotropy and dipolar energies are all symmetric with respect to the permutation of two neighboring spins, Bloch DWs with left- or right-handed chirality are randomly distributed, so the system on average, is achiral. However, at surfaces or interfaces where inversion symmetry is broken, the antisymmetric Dzyaloshinskii–Moriya interaction (DMI) [2, 3] can stabilize Néel DWs with fixed chirality [4]. Such chiral spin textures, in the form of spin spirals [5, 6] or magnetic skyrmions [7–9], can be driven by electrical currents with extremely high efficiency [10–14], making them promising for future spintronic memory or logic devices [15, 16]. The Néel-type chiral spirals have been imaged by advanced microscopic methods like spin-polarized scanning tunneling microscopy [5] or spin-polarized low energy electron microscopy [6]. The current-driven DW motion was typically captured by magneto-optical Kerr microscopy [13, 14]. However, electrical transport signatures have rarely been reported.

* Author to whom any correspondence should be addressed.

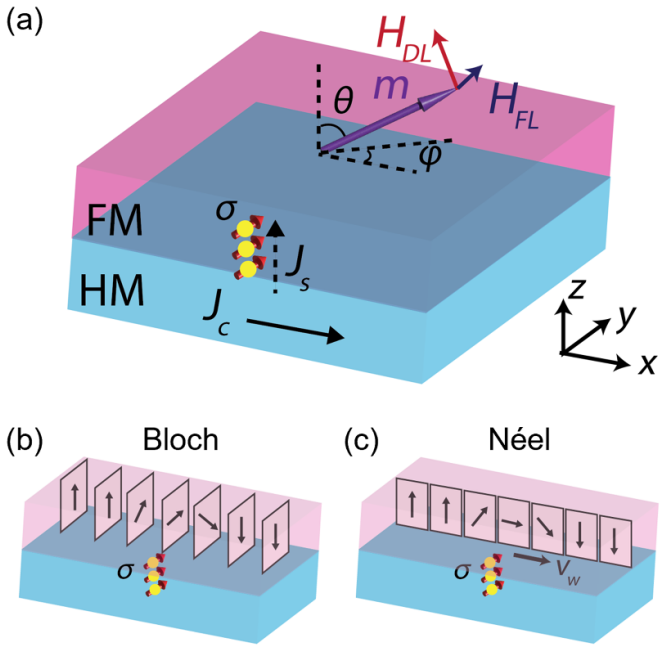

Figure 1. (a) Schematic of the second-harmonic Hall voltage SOT measurement mechanism. The injected spin current from the HM generates damping-like (H_{DL}) and field-like (H_{FL}) effective fields, which rotates the single domain magnetization and modifies the anomalous and planar Hall resistances of the FM layer. Such current-induced modification of resistance can be measured as a second-harmonic Hall voltage. (b) In the Bloch-type domain wall, the net magnetization is parallel to the injected spin polarization direction $\boldsymbol{\sigma}$, so SOT has no effect on the DW. (c) In the Néel-type domain wall, the net magnetization is perpendicular to $\boldsymbol{\sigma}$. The domain wall acquires a velocity under SOT.

The second-harmonic Hall voltage (SHV) measurement method [17, 18] has been frequently used to calibrate the magnitude of spin–orbit torques (SOTs) in heavy metal/ferromagnet (HM/FM) heterostructures. The principle is based on current-induced change in the anomalous or planar Hall (AH or PH) resistance of the FM layer. As sketched in figure 1(a), the charge current flowing in the x-direction in the HM can generate net spin accumulation polarized in the y-direction. The damping-like (DL) effective field $\boldsymbol{H}_{\mathrm{DL}} \propto \boldsymbol{m} \times \boldsymbol{\sigma}$ and field-like (FL) effective field $\boldsymbol{H}_{\mathrm{FL}} \propto \boldsymbol{\sigma}$ will coherently rotate the magnetization, so the AH and PH resistances are modified, which can be detected as a SHV response. Here $\boldsymbol{m}$ is the unit vector of the magnetization direction and $\boldsymbol{\sigma}$ denotes the spin polarization direction. The critical assumption for this model is that the magnetization of the FM layer is saturated in a single-domain state, therefore SOTs only rotate the magnetization. The SHV responses in the multidomain regime are typically ignored. As shown in figure 1(b), Bloch DWs are immobile under SOT because the net magnetization of the wall is parallel to $\boldsymbol{\sigma}$. However, as illustrated in figure 1(c), the net magnetization of Néel DWs is perpendicular to $\boldsymbol{\sigma}$, and the DL SOT can efficiently drive the DWs [19].

In this study, we tuned the magnetic anisotropy of W/Pt/Co films so that potential Néel-type DWs can be stabilized by the interfacial DMI. Anomalous SHV 'humps' were observed in the out-of-plane (OP) to in-plane (IP) spin-reorientation transition brought out by sweeping the external magnetic field. We extended the analysis to the multidomain regime and interpret these humps as a second-harmonic signature of chiral Néel DWs efficiently driven by the small SOTs in the W/Pt/Co heterostructures.

2. Methods

The W(0–3 nm)/Pt(0–3 nm)/Co(0.8–1.4 nm) films were deposited on thermally oxidized silicon wafers at room temperature in a home-built magnetron sputtering chamber with base pressure $\sim 3 \times 10^{-7}$ Torr. All films were capped with 5 nm thick SiO_2 to avoid oxidation. X-ray diffraction (XRD) measurements were performed in a Rigaku diffractometer with a copper K-α radiation source. The Hall bar devices with channel dimension 50 $\times$ 10 μm were fabricated by the standard photolithography method. Magneto-transport measurements were performed mostly in a home-built setup and partially in a Quantum Design physical property measurement system. Sinusoidal a.c. currents with a frequency of 346.1 Hz were generated by a Keithley 6221 current source, and the first- and second-harmonic voltages were collected by Stanford Research SR830 lock-in amplifiers. Films for magnetic force microscopy (MFM) imaging were precoated with 5 nm Pt to avoid the accumulation of static charges. The low-temperature MFM measurements were carried out in a homemade variable-temperature MFM system using commercial piezoresistive cantilevers with a resonant frequency $f_0 \approx 43$ kHz and a spring constant $k \approx 3$ N m^{-1}. MFM tips were deposited with nominally 100 nm Co by using magnetron sputtering. MFM images were taken using constant-height

non-contact mode with MFM tip scanning on a plane that is ∼70 nm above the sample surface. The shift of the cantilever resonant frequency (MFM signal), which is proportional to the out-of-plane stray field gradient, was extracted using a commercial phase-locked loop (Nanonis^{TM}).

3. Results and discussion

3.1. Tuning magnetic anisotropy in W/Pt/Co

In our experiments, we find the W buffer layer is crucial for promoting the PMA in the W/Pt/Co heterostructures. To check the role of the W layer, we prepared two 55 nm thick Pt films, one directly on a silicon wafer and the other on a 3 nm W buffer layer on top of the wafer. As plotted in figure 2, the XRD results show that the direct deposition on silicon wafer results in a mixed (111) and (311) oriented Pt polycrystalline structure, while with a W buffer layer, the undesired (311) phase is significantly suppressed. This suggests that the W buffer layer helps promote the (111) Pt phase at the W/Pt interface, resulting in an enhanced PMA at the Pt/Co interface. This shares the same mechanism with the previously studied Ta/Pt/Co [20] and Ti/Pt/Co [21] multilayers.

The magnetic anisotropy of W/Pt/Co films with varying W, Pt, or Co thicknesses was examined by anomalous Hall effect (AHE) measurements with magnetic field applied perpendicular to the film plane (figure 3(a)). As shown in figure 3(b), without the W buffer layer, the easy-axis of Pt(3)/Co(1.1) (number in nanometers, same hereafter) is in-plane. Inserting only a 1 nm thick W buffer between the Pt layer and the substrate significantly reduces the in-plane anisotropy, and a 3 nm W buffer layer induces robust PMA revealed by the nearly 100% squareness of the hysteresis loop. Figure 3(c) shows that the W/Co bilayer has an in-plane easy axis, with a large anisotropy field of over 10 kOe. The Pt/Co interface is essential for the PMA because of the enhanced Co orbital moment due to interfacial hybridization [22, 23]. The interfacial nature of the PMA is demonstrated by varying Co thickness (figure 3(d)). When the Co layer changes from 0.8 to 1.4 nm, the easy axis gradually changes from out-of-plane to in-plane. We have demonstrated the robust and tunable magnetic anisotropy in W/Pt/Co can be achieved by room temperature sputter-deposition, without any requirement of epitaxial growth, special oxide capping layers or further annealing treatment.

3.2. Transport signature of chiral spin structures

Hayashi *et al* [18] developed the SHV method to calibrate the magnitude of SOTs in in-plane magnetized systems. As illustrated in figure 4(a), in most of our measurements the external magnetic field is applied in a nearly normal direction with a finite tilt angle θ_H. The first and second harmonic Hall voltages as a function of external magnetic field for three W/Co or W/Pt/Co samples with distinct magnetic anisotropy are plotted in figures 4(b)–(d). The small tilt angle is necessary to give a well-defined x-direction polarity for the magnetization. In our experiments magnetic field H is always applied in the xz plane and due to the small in-plane anisotropy of most HM/FM systems, the in-plane component of magnetization follows that of H. Under these conditions, the SHV is given as [18]

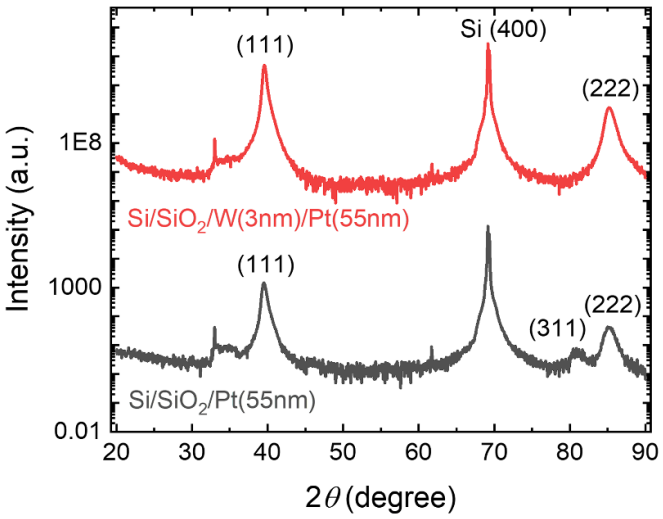

Figure 2. XRD results of Pt(55 nm) and W(3 nm)/Pt(55 nm) films deposited on thermally oxidized silicon wafers.

$$V_y^{2\omega} = -R_{\mathrm{AHE}}\left[\frac{1}{2}\frac{H_{\mathrm{DL}}\sin\theta}{H_k\cos 2\theta + H\cos(\theta_H-\theta)} + \frac{R_{\mathrm{PHE}}}{R_{\mathrm{AHE}}}\frac{H_{\mathrm{FL}}\sin^2\theta}{-H_a\sin\theta + H\sin\theta_H}\right]I_0, \quad (1)$$

where R_{AHE} and R_{PHE} are the AH and PH resistances, respectively; I_0 is the magnitude of the sinusoidal current; θ gives the equilibrium position of the magnetization $\boldsymbol{m}$; H, H_k and H_a are the external, out-of-plane and in-plane anisotropy fields, respectively; and H_{DL} and H_{FL} denote the DL and FL effective fields, respectively. As exemplified by the W(3)/Co(1.1) sample (figure 4(b)), in typical HM/FM systems where the easy-axis lies in the sample plane, as H decreases from above H_k (∼12 kOe) to zero, $V_y^{2\omega}$ typically increases monotonically, following more or less a $1/H$ type trend. For out-of-plane magnetized systems with robust PMA, $\theta = 0$ so there is no SHV response. This is indeed the case for the W(3)/Pt(1)/Co(0.8) sample (figure 4(c)). However, in the W(3)/Pt(1)/Co(1.1) device (figure 4(d)), where the easy-axis is mostly in-plane but with a small out-of-plane component (confirmed by in-plane PHE measurements), as H decreases from 2 kOe to zero, $V_y^{2\omega}$ develops a hump in the intermediate field region where the magnetic moments are oriented from out-of-plane to in-plane direction. We note that the model of equation (1) only considers the rotation of magnetization by SOTs. The unusual hump feature in the W(3)/Pt(1)/Co(1.1) sample is likely to have another origin, i.e. current-driven DW motion as described in the introduction.

The temperature evolution of the first-harmonic AHE and second-harmonic SOT voltages of the W(3)/Pt(1)/Co(1.1) sample under a nearly normal magnetic field is summarized

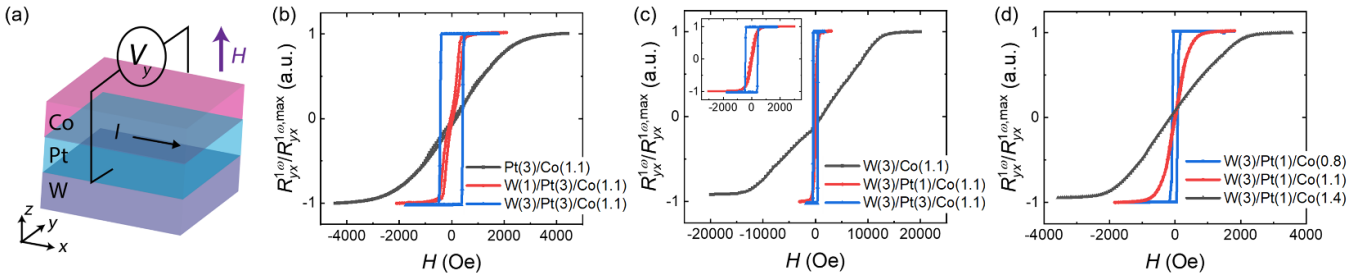

Figure 3. (a) Illustration of the AHE measurement setup. (b)–(d) Normalized AH resistance as a function of out-of-plane magnetic field for W/Pt/Co devices with different W, Pt, and Co thicknesses. All measurements were performed at room temperature.

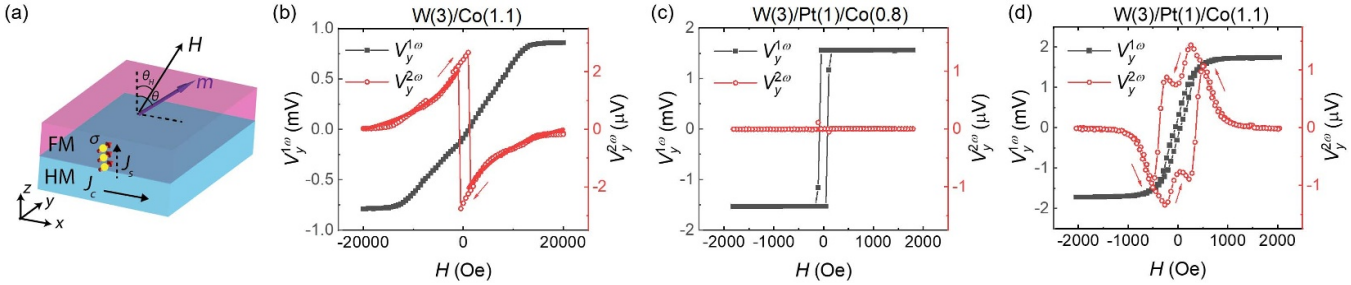

Figure 4. (a) Schematic of the Hall voltages measurement setup. The external magnetic field H is nearly to the out-of-plane direction, with a small tilt angle of $\theta_H \sim 3°$. (b)–(d) First- and second-harmonic Hall voltages as a function of external magnetic field for the W(3)/Co(1.1) (b), W(3)/Pt(1)/Co(0.8) (c), and W(3)/Pt(1)/Co(1.1) (d) devices. All measurements were performed at room temperature with a 0.6 mA current. The red arrows in (b) and (d) indicate field sweep directions for the $V_y^{2\omega}$ loops. The red solid lines in (b) is a $1/H$ type fit working as a guide for the eye.

in figure 5. Interestingly, as the temperature decreases from 290 K to 50 K, the in-plane anisotropy becomes stronger, and the AHE hysteresis loop gradually develops a wasp-waist feature (figure 5(a)). Such sheared hysteresis resemble those in magnetic multilayers where spin spirals or skyrmions typically form [24, 25]. As shown in figure 5(b), at and below 150 K, the central SHV response around zero field decreases to almost zero. This is probably because in the W/Pt bilayer the Pt spin diffusion length increases as temperature drops, so the overall spin Hall angle (SHA) is reduced from 0.03 at 290 K to being negligible below 150 K, as checked by in-plane SHV measurements. The height of the humps also decreases and their position shifts to higher field regions. Importantly, the humps always appear in the same field regime with the sheared AHE hysteresis. To better illustrate this, we plotted the HT phase diagrams for the slope of the AHE voltage $dV_y^{1\omega}/dH$ and the SHV $V_y^{2\omega}$. As shown in figures 5(c) and (d), $dV_y^{1\omega}/dH$ and $V_y^{2\omega}$ take maximum values in the same HT phase space regions. This suggests the DW formation during the out-of-plane to in-plane spin-reorientation phase transition plays a critical role in generating the anomalous SHV responses.

Based on the above results, we draw the physical picture for the SHV hysteresis as shown in figure 6. The out-of-plane magnetic field induces metamagnetic phase transition which can be distinguished from the AHE loop as out-of-plane ferromagnet (OP FM), Néel DW, and in-plane ferromagnet (IP FM) regimes (figure 6(a)). In the OP FM regime, as discussed for the PMA sample in figure 4(c), the derivative of magnetization $\boldsymbol{M}$ to current I is zero, so there is no SHV response. In the IP FM regime, SOT only works to rotate the magnetization. At 120 K, the spin currents from the W and Pt layers with opposite SHAs nearly cancel each other, so SHV is barely detectable. However, during the out-of-plane to in-plane transition, clear SHV humps emerge, demonstrating that the magnetization is modified by the nevertheless small SOT, not by rotation, but by DW motion. As illustrated in figure 6(b), this can only happen for Néel-type DWs. Bloch walls have no response to SOTs, but Néel walls can be efficiently driven by the DL effective field. Moreover, Néel walls with the same chirality will move in the same direction, giving no change to M_z. Therefore, a finite in-plane magnetic field component is required to break the left- or right-handedness degeneracy, so the out-of-plane magnetized domains, bounded by Néel walls with opposite chirality, will expand or contract under SOT. As a result, this current-induced change in M_z is reflected as the SHV humps in this transition regime.

To support our claim, we carried out SHV measurements on the W(3)/Pt(1)/Co(1.1) sample with different field-sweep angles. As plotted in figure 7, indeed when the angle θ_H changes from $-5°$ to $5°$, the hysteresis changes sign. This is because the opposite x-direction magnetic field component

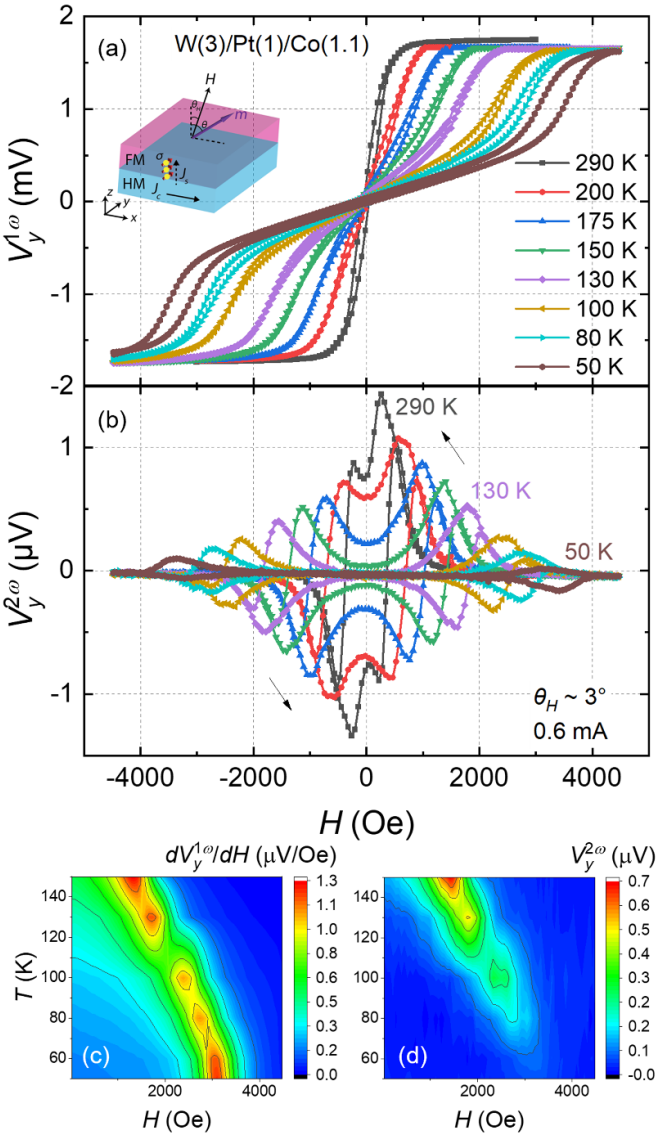

Figure 5. (a) and (b) First- and second-harmonic Hall voltages as a function of out-of-plane magnetic field scans with a small tilt angle $\theta_H \sim 3^\circ$ between 50 and 290 K for the W(3)/Pt(1)/Co(1.1) sample. The arrows in (b) indicate field sweep directions. (c) and (d) Contour plots of the slope of the first-harmonic AHE voltage $dV_y^{1\omega}/dH$ and the second-harmonic voltage $V_y^{2\omega}$ between 50 K to 150 K in a magnetic field range of 0–4500 Oe.

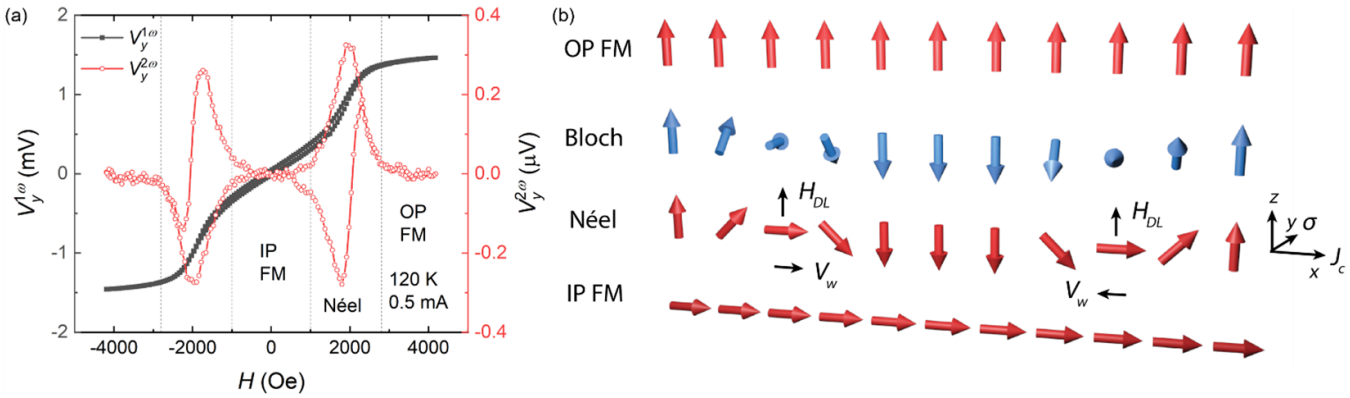

Figure 6. (a) First- and second-harmonic Hall voltages as a function of OP magnetic field with a small tilt angle $\theta_H \sim 3^\circ$ at 120 K for the W(3)/Pt(1)/Co(1.1) device. (b) Illustration of the SOT effects on IP and OP magnetic domains in the saturated FM state, and Bloch- and Néel-type domain walls. Only Néel DWs can be efficiently driven by damping-like effective field H_{DL}.

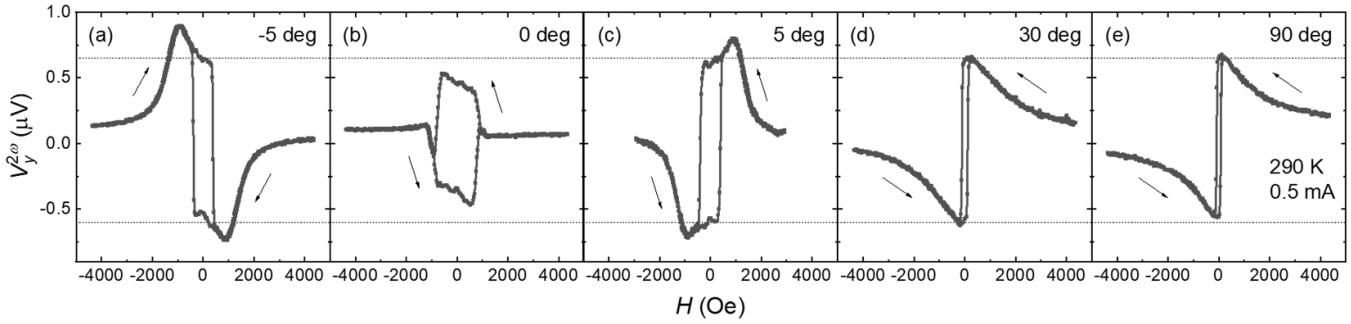

Figure 7. Field-angle dependence of the SHV in the W(3)/Pt(1)/Co(1.1) sample. The magnetic field H takes different angles θ_H in the x–z plane, as defined in figure 4(a). The black arrows indicate field sweep directions. The dashed lines indicate the zero field $V_y^{2\omega}$ value remains almost the same for different sweeping angles except 0 degree.

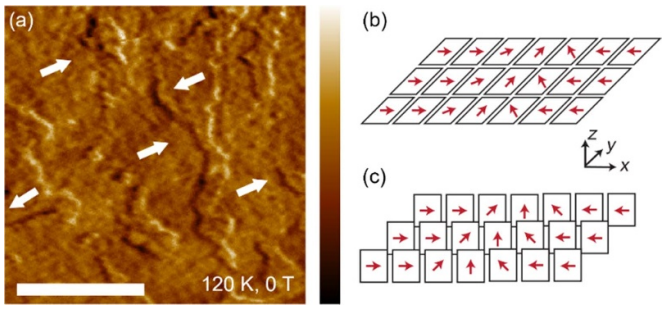

Figure 8. (a) MFM stray field strength map of the W(3)/Pt(1)/Co(1.1) sample at 120 K under zero magnetic field. The white arrows denote inferred magnetization direction in each domain. The dimension scale bar is 10 μm and the color scale bar for MFM is 240 mHz. (b) and (c) Domain walls with in-plane (b) and out-of-plane (c) net magnetization.

favors opposite chirality, so the SOT effects are opposite. At $\theta_H = 0$, there are equal amount of left- and right-handed DWs, the overall domain wall motion averages out, so the SHV loop collapses. When H is applied in the in-plane direction ($\theta_H = 90°$), there is no out-of-plane to in-plane spin-reorientation transition, so there are no Néel DWs to give the hump features. We notice that except at $\theta_H = 0$, the SHV under zero magnetic field takes a constant value regardless of the field sweep angles.

To explain this constant $V_y^{2\omega}$ at zero field, we carried out MFM measurements under zero magnetic field for this W(3)/Pt(1)/Co(1.1) film after saturating it by placing it on top of a permanent magnet. Figure 8(a) shows typical MFM result at 120 K. Stripe domains with alternating bright and dark lines are observed. These line features are likely head-to-head or tail-to-tail DWs [26], indicating domains with in-plane magnetization labeled by arrows in figure 8(a). Based on the stray field distribution, there are two possible DW configurations: the regular IP type (figure 8(b)) and the chiral OP type (figure 8(c)). However, neither of them gives rise to a SHV response due to SOT-driven DW motion. In the former case, the DWs are immobile under SOT. In the latter case, although the DWs can be driven by DL-SOT, but the overall net x, y, or z magnetization component of the Co layer does not change, so in the in-plane magnetized regime, the only contribution to the SHV is the SOT-driven rotation mechanism. Therefore, when the W(3)/Pt(1)/Co(1.1) sample is mostly magnetized in the in-plane direction, regardless of its different domain configuration in different field-sweeping angles, $V_y^{2\omega}$ takes the same value around zero field.

4. Conclusion

In summary, we utilized the W buffer layer to tune the magnetic anisotropy at the Pt/Co interface. The large DMI [27, 28] at this interface also allows the formation of Néel-type DWs, when the external magnetic field is applied to induce a spin spiral state with out-of-plane magnetized background. These Néel DWs can be efficiently driven by SOT. When there is a finite in-plane magnetic field component to break the chiral degeneracy, the current-driven DW motion will cause a change of M_z in Co, which is detected as large humps in the SHV hysteresis. Our results extend the interpretation of the SHV data to the multidomain regime, which serves as a signature of chiral spin structures in magnetic multilayers exhibiting inversion symmetry breaking and large spin-orbit interaction. This specific W/Pt/Co heterostructure with robustly tunable magnetic anisotropy and SHA, and substantial DMI, is a fruitful platform to study various spintronic phenomena ranging from magnetic anisotropy, SOT, to chiral spin textures.

Data availability statement

All data that support the findings of this study are included within the article (and any supplementary files).

Acknowledgments

We thank Y Ji for use of the cryogenic transport measurement system, and X Chen and A Soumyanarayanan for helpful discussions. The work at Delaware was supported by NSF under Grant No. NSF DMR 1904076. The MFM measurements at Rutgers were supported by the Office of Basic Energy Sciences, Division of Materials Sciences and Engineering, U.S. Department of Energy under Award No. DE-SC0018153. The work at Bryn Mawr College was supported by NSF under Grant No. NSF DMR 1708790.

ORCID iD

John Q Xiao https://orcid.org/0000-0001-7805-8155

References

[1] Hubert A and Schäfer R 1998 *Magnetic Domains: The Analysis of Magnetic Microstructures* (Berlin: Springer)

[2] Dzyaloshinsky I 1958 A thermodynamic theory of "weak" ferromagnetism of antiferromagnetics *J. Phys. Chem. Solids* **4** 241–55

[3] Moriya T 1960 Anisotropic superexchange interaction and weak ferromagnetism *Phys. Rev.* **120** 91

[4] Heide M, Bihlmayer G and Blügel S 2008 Dzyaloshinskii-Moriya interaction accounting for the orientation of magnetic domains in ultrathin films: Fe/W(110) *Phys. Rev.* B **78** 140403(R)

[5] Bode M, Heide M, von Bergmann K, Ferriani P, Heinze S, Bihlmayer G, Kubetzka A, Pietzsch O, Blügel S and Wiesendanger R 2007 Chiral magnetic order at surfaces driven by inversion asymmetry *Nature* **447** 190

[6] Chen G *et al* 2013 Novel chiral magnetic domain wall structure in Fe/Ni/Cu(001) films *Phys. Rev. Lett.* **119** 177204

[7] Yu X Z, Onose Y, Kanazawa N, Park J H, Han J H, Matsui Y, Nagaosa N and Tokura Y 2010 Real-space observation of a two-dimensional skyrmion crystal *Nature* **465** 901

[8] Heinze S, von Bergmann K, Menzel M, Brede J, Kubetzka A, Wiesendanger R, Bihlmayer G and Blügel S 2011 Spontaneous atomic-scale magnetic skyrmion lattice in two dimensions *Nat. Phys.* **7** 713

[9] Huang S X and Chien C L 2012 Extended skyrmion phase in epitaxial FeGe(111) thin films *Phys. Rev. Lett.* **108** 267201

[10] Moore T A, Miron I M, Gaudin G, Serret G, Auffret S, Rodmacq B, Schuhl A, Pizzini S, Vogel J and Bonfim M 2008 High domain wall velocities induced by current in ultrathin Pt/Co/AlO_x wires with perpendicular magnetic anisotropy *Appl. Phys. Lett.* **93** 262504

[11] Miron I M *et al* 2011 Fast current-induced domain-wall motion controlled by the Rashba effect *Nat. Mater.* **10** 419–23

[12] Thiaville A, Rohart S, Jué É, Cros V and Fert A 2012 Dynamics of Dzyaloshinskii domain walls in ultrathin magnetic films *Europhys. Lett.* **100** 57002

[13] Haazen P P J, Mure E, Franken J H, Lavrijsen R, Swagten H J M and Koopmans B 2013 Domain wall depinning governed by the spin Hall effect *Nat. Mater.* **12** 299–303

[14] Emori S, Bauer U, Ahn S M, Martinez E and Beach G S 2013 Current-driven dynamics of chiral ferromagnetic domain walls *Nat. Mater.* **12** 611

[15] Parkin S S P, Hayashi M and Thomas L 2008 Magnetic domain-wall racetrack memory *Science* **320** 190

[16] Hayashi M, Thomas L, Moriya R, Rettner C and Parkin S 2008 Current-controlled magnetic domain-wall nanowire shift register *Science* **320** 209

[17] Pi U H, Kim K W, Bae J Y, Lee S C, Cho Y J, Kim K S and Seo S 2010 Tilting of the spin orientation induced by Rashba effect in ferromagnetic metal layer *Appl. Phys. Lett.* **97** 162507

[18] Hayashi M, Kim J, Yamanouchi M and Ohno H 2014 Quantitative characterization of the spin-orbit torque using harmonic Hall voltage measurements *Phys. Rev.* B **89** 144425

[19] Khvalkovskiy A V, Cros V, Apalkov D, Nikitin V, Krounbi M, Zvezdin K A, Anane A, Grollier J and Fert A 2013 Matching domain-wall configuration and spin-orbit torques for efficient domain-wall motion *Phys. Rev.* B **87** 020402

[20] Zhang W, Jia X, Wang R, Liu H, Xiao Z, Quan Z and Xu X 2020 The influence of an ultra-high resistivity Ta underlayer on perpendicular magnetic anisotropy in Ta/Pt/Co/Pt heterostructures *RSC Adv.* **10** 11219

[21] Ocal M T, Sakar B, Oztoprak I, Balogh-Michels Z, Neels A and Ozturk O 2021 Structural and morphological effect of Ti underlayer on Pt/Co/Pt magnetic ultra-thin film *Jpn J. Appl. Phys.* **60** 105505

[22] Carcia P F, Meinhaldt A D and Suna A 1985 Perpendicular magnetic anisotropy in Pd/Co thin film layered structures *Appl. Phys. Lett.* **47** 178

[23] Nakajima N, Koide T, Shidara T, Miyauchi H, Fukutani H, Fujimori A, Iio K, Katayama T, Nývlt M and Suzuki Y 1998 Perpendicular magnetic anisotropy caused by interfacial hybridization via enhanced orbital moment in multilayers: magnetic circular x-ray dichroism study *Phys. Rev. Lett.* **81** 5229–32

[24] Soumyanarayanan A *et al* 2017 Tunable room-temperature magnetic skyrmions in Ir/Fe/Co/Pt multilayers *Nat. Mater.* **16** 898

[25] Chen X, Chue E, Kong J F, Tan H R, Tan H K and Soumyanarayanan A 2022 Thermal evolution of skyrmion formation mechanism in chiral multilayer films *Phys. Rev. Appl.* **17** 044039

[26] Rugar D, Mamin H J, Guethner P, Lambert S E, Stern J E, McFadyen I and Yogi T 1990 Magnetic force microscopy: general principles and application to longitudinal recording media *J. Appl. Phys.* **68** 1169–83

[27] Di K, Zhang V L, Lim H S, Ng S C, Kuok M H, Yu J, Yoon J, Qiu X and Yang H 2015 Direct observation of the Dzyaloshinskii–Moriya interaction in a Pt/Co/Ni film *Phys. Rev. Lett.* **114** 047201

[28] Belmeguenai M, Adam J P, Roussigné Y, Eimer S, Devolder T, Kim J V, Cherif S M, Stashkevich A and Thiaville A 2015 Interfacial Dzyaloshinskii-Moriya interaction in perpendicularly magnetized Pt/Co/AlO_x ultrathin films measured by Brillouin light spectroscopy *Phys. Rev.* B **91** 180405